J. Biomater. Sci. Polymer Edn, Vol. 13, No. 3, pp. 337–348 (2002)

An atomic force microscopic study of the ultrastructure of dental enamel afflicted with *amelogenesis imperfecta*

N. BATINA [1], V. RENUGOPALAKRISHNAN [2,3,*], P. N. CASILLAS LAVÍN [4], JUAN CARLOS HERNÁNDEZ GUERRERO [4], M. MORALES [1] and R. GARDUÑO-JUÁREZ [5]

[1] *Depto. de Química, Universidad Autónoma Metropolitana, Iztapalapa 09340, México DF, Mexico*
[2] *Children's Hospital, Harvard Medical School, Boston, MA 02115, USA*
[3] *BioFold Inc., 650 Saratoga Ave., San Jose, CA 95129, USA*
[4] *Faculty of Dentistry, Universidad Nacional Autónoma de México, 04510 México DF, Mexico*
[5] *Centro de Ciencias Físicas, Universidad Nacional Autónoma de México, 62210 Cuernavaca, Morelos, Mexico*

Received 21 November 2001; accepted 13 February 2002

Abstract—The ultrastructure of human tooth enamel from a patient diagnosed to have *amelogenesis imperfecta* (AI) was investigated using atomic force microscopy (AFM) and compared with normal human tooth enamel. AI is a hereditary defect of dental enamel in which the enamel is deficient in either quality or quantity. Tissue-specific proteins, especially amelogenins, have been postulated to play a central role in amelogenesis. The secondary structure of amelogenin has been assigned an important role in directing the architecture of hydroxyapatite (HA) enamel crystallites and an alteration of the secondary structure of amelogenin is expected to result in an altered architecture of the mineral phase in human enamel. Previous studies have shown that the human amelogenin gene encodes for a mutant protein in which a conserved Pro is mutated to a Thr residue (Pro → Thr); such a mutation should be expected to cause a disoriented pattern of the mineral phase in enamel. AFM results presented for the AI tooth enamel clearly demonstrate that the apatite crystal morphology in AI tooth enamel is perturbed in the diseased state; this might result from a defective synthesis of the extracellular matrix proteins, e.g. amelogenin, by the ameloblasts.

Key words: *Amelogenesis imperfecta*; atomic force microscopy; tooth enamel surface; surface morphology of tooth enamel; ultrastructure.

*To whom correspondence should be addressed. BioFold Inc., 650 Saratoga Ave., San Jose, CA 95129, USA. Fax: + 1.408.557.6799. E-mail: Renu@biofold.net

INTRODUCTION

Enamel is a bioceramic and is distinguished from other mineralized tissues such as bone in at least two important aspects. First, unlike bone, enamel is not remodelled continuously throughout its life span and its extracellular matrix is almost completely removed concomitantly with the mineralization process. Second, the resulting mineral phase in healthy tooth enamel is comprised of a highly-ordered packing of hydroxyapatite (HA) crystallites, more than ten times larger than those of bone, organized into discrete substructures, 'prisms', in which the individual crystallites are collectively oriented with their *c*-axes essentially normal to the plane of the dentin–enamel junction.

It is well accepted that the tissue-specific proteins of the developing dental enamel, amelogenins, provide the extracellular matrix which is essential for the formation of the unique enamel mineral phase. Amelogenins [1–3] from a number of species have been isolated, characterized, purified, cloned, and expressed in *Escherichia coli*. The secondary structure of amelogenin has been postulated to orchestrate the mineralization process in enamel. The precise mechanisms underlying the mineralization process are not completely understood at present. Nevertheless, it is clear that these unique tissue-specific proteins play a central role in amelogenesis. The secondary structure of bovine amelogenin [4], consisting of β-sheet/β-turns and with a low α-helical content, contains a unique β-spiral structure in the core and was derived from circular dichroism (CD), Fourier transform infrared (FT-IR) [5] and Raman spectroscopic studies [6], and molecular mechanics-dynamics refinement from nuclear Overhauser (NOE) contacts from three-dimensional (3D) NMR studies [7–9].

Since then, the 3D structure of bovine amelogenin from multi-nuclear NMR has been refined (Renugopalakrishnan *et al*., submitted). Recently we have also derived the tentative secondary structure of 179-reside recombinant mouse amelogenin from CD and FT-IR studies and its thermal unfolding was investigated using CD and differential scanning calorimetric (DSC) studies from our laboratories (Oobatake *et al*., submitted; Renugopalakrishnan *et al*., submitted). The secondary structures of bovine, mouse, and human amelogenins appear to share common secondary structural motifs, despite differences in their primary structures [2].

Amelogenin regulates the formation of HA crystals in the mineralization of enamel in a manner that is yet to be resolved. The 3D architecture of mineral, manifest in the shape of hexagonal prisms of HA, has been observed in the electron micrographs of mature enamel [10]. A defective human amelogenin gene has been shown to encode a mutant version of the protein [11] and the X-chromosomal amelogenin gene appears to be a candidate gene for X-linked *amelogenesis imperfecta* (AI). AI is a hereditary defect of dental enamel in which the enamel is deficient in either quality or quantity [12]. The mutant protein should be expected to have an altered 3D structure due to the mutation of a conserved Pro to Thr and such a mutation should be expected to distort the β-spiral segment, which is a dominant structural component in bovine amelogenin [5] and could result through

a cascade of events which are still incompletely understood in a poorly oriented mineral architecture due to impairment of the sequestering of Ca^{2+}.

There have been a few reports in the literature of scanning electron microscopic (SEM) studies of the surface characteristics of enamel [13–15]. A SEM study of hypoplastic-type AI in primary teeth has been reported by Uzamis *et al*. [16].

The present study is the first report in the literature on the ultrastructure of human tooth enamel from normal patients and patients diagnosed to have AI using atomic force microscopy (AFM). Other researchers [17, 18] have presented the results of an AFM study of dimensional changes in human dentin. Recently there has been a preliminary report using AFM to study tooth surfaces [14] and another AFM study of the dentin–enamel junction [16].

MATERIALS AND METHODS

Preparation of human tooth enamel specimens and clinical diagnosis

The first sample was derived from the third lower molar from a male patient, 25 years old, with no dental abnoramalities (NA).

The second sample was derived from the lower first primary molar of a female child, 7 years old, with normal oral health, i.e. no dental abnormalities (NC).

The third sample was derived from the upper first permanent molar of a female child, 7.5 years old, clinically diagnosed to have AI. The girl was a patient at the Pedodontic Clinic at the Postgraduate and Research Studies Division, Dental School of the National Autonomous University of Mexico in Mexico City. The clinical history of this patient shows a normal health; however, her mother was concerned about yellowing of the teeth and their sensitivity to thermal changes. On further research into her familial history, it was learned that her father's cousin also manifested the same dental features. On intra-oral examination, the patient was found to have mixed dentition; most teeth were yellow with a smooth surface and the rest possessed rough surfaces with loss of enamel cover. The teeth were found to be free of caries. Panoramic radiography showed irregular contours in the crown of all teeth with ill-defined enamel limits. The pulp chambers were thick and long. All the features manifested were indicative of a diagnosis pointing to hypomaturation–hypoplasia AI with taurodontism. The sample used in this study was detached with an explorer from the buccal surfaces of the first upper molar.

Tooth specimen samples, pellicle-free, were plates of 1 mm $\times$ 1 mm (length and width) and around 2 mm thick. After polishing the rear of the sample to be fixed on the flat AFM sample holder, the samples were rinsed in ethanol (5 min in ultrasonic bath) and then rinsed again with ethanol. Before imaging, all samples were rinsed with ultra-pure Millipore water. It is important to point out that the sample did not require any special preparation. We were careful to remove grease from the sample surface, and polishing on the rear of the sample to hold it in the sample holder. From each tooth specimen, we dissected two samples and each was imaged at five different places.

We used a large number of tooth specimens to ensure that the results were consistent; there were no significant changes between tooth specimens within a class.

AFM studies

The surface morphology of the tooth samples was probed by a commercial atomic force microscope (AFM), Nanoscope III (Digital Instruments, Santa Barbara, CA, USA). Imaging was performed *ex situ*, under controlled temperature and humidity. AFM was operated in 'contact' and 'tapping' modes (Digital Instruments, manual for Nanoscope III-SPM) [19]. We scanned a tooth specimen surface of $10 \times 10\ \mu$m. These two modes differ in terms of physical contact between the AFM probe (tip) and the imaged surface. In the 'contact' mode, physical contact between the tooth surface and the AFM tip was maintained constantly and with a constant force. The 3D motion of the cantilever and AFM tip attached to the piezo corresponds to the surface morphology of the scanned area. Imaging was performed with standard geometry silicon nitride probes. AFM images were collected at a very slow scan rate of 1 Hz, in order to obtain details of the enamel structure and to avoid damaging the tip.

'Tapping' mode imaging is a more sophisticated type of measurement, in which the tip contacts the image surface at regular intervals, but does not establish permanent contact. Such imaging is recommended for more sensitive samples, which could be damaged during the tip rastering process. Another advantage of 'tapping' mode imaging is the possibility to collect height, amplitude, and phase type data. As we will demonstrate later in this paper, such extensive and sophisticated AFM analyses helped us to visualize structural details of the different features found at the tooth surface. Shortly before imaging by both methods, all samples were regularly rinsed with ultrapure water and dried in a stream of air. We used an optical stereo-microscope to choose up to five different places for AFM imaging on each sample.

The images presented in this paper are mostly plotted in the 'height mode', which is typical for the presentation of surface topography. The higher part of the surface appears brighter in the 2D or 3D image. The tapping mode data (amplitude and phase imaging) are presented in 2D 'top-view' mode.

RESULTS AND DISCUSSION

The observed tooth morphological characteristics are described qualitatively and quantitatively. For quantitative evaluation, only the 'height' mode imaging data and the software package for image analysis, available with the Nanoscope 111-AFM instrument, were used. To satisfy the statistical nature of the quantitative analysis, images were collected from a variety of different places on the tooth specimens; several samples of each kind, collected from different patients, were also used.

As described in the Materials and Methods section, the surface morphology of the outer part of the human tooth (enamel) was studied using normal healthy teeth from an adult (NA) and child (NC), and teeth from a child with *amelogenesis imperfecta* (AIC). Each sample was analyzed in terms of surface topography, spatial arrangement, surface roughness, and surface feature characterization, i.e. size and shape of the surface features.

AFM surface morphology analysis of the normal healthy tooth

In order to learn how to differentiate the major morphological characteristics of the outer surface of enamel for the different samples (healthy and AI teeth), we will first focus on the characterization of the healthy teeth from the adult (NA) and child (NC).

The AFM images presented in Figs 1a and 1b show the top surface of the enamel of the NA tooth. Images were collected using the 'tapping' mode technique and are presented in the 'height' (Fig. 1a) and 'amplitude' (Fig. 1b) mode. From the 'height mode' image, one can observe that the tooth surface consists mainly of two kinds of grains: small ones (average diameter from 0.2 to 0.5 μm) which are somehow incorporated in/associated with large associates with an average diameter of 2–4 μm. It is difficult to discern any order of grain alignment. However, one can clearly see that the grains are closely touching each other. In particular, the small grains and their relationship to the larger associates can be clearly recognized in the AFM image recorded in the 'tapping amplitude' mode (Fig. 1b). This image clearly reveals the compact packing between the apatite grains during the enamel formation. In several samples, we also estimated the average surface roughness of the imaged surface. For the NA tooth, the RMS (Rq) (root-mean-square roughness [20–23]), a normal measure used to express the surface roughness, was estimated to be 116.50 nm. The RMS (Rq) was calculated from a complete AFM image. The real meaning and the value of this analysis will be discussed later, in comparison with other surfaces.

Figure 2 shows the AFM image of the healthy child tooth (NC). The image was recorded under identical conditions to Fig. 1 and is also presented in both 'height' (Fig. 2a) and 'amplitude' (Fig. 2b) modes. In comparison to the NA tooth, we can observe that the surface of the NC tooth is much more uniform and significantly smoother. From Fig. 2b, it is possible to observe that most of the grains possess a similar (triangular) shape and size (0.25–0.3 μm). Although rare, we can also see that at some segments of the image, the grains are aligned in rows. On the other hand, there are infrequent occurrences of regular grains forming aggregates consisting of 5–20 units. The surface of the NC tooth appears to be much more smoother than that of the NA tooth. The RMS (Rq) was found to be 48.8 nm. Again, as in the NC tooth, grains were found to be closely packed, with no pores on the enamel surface. The 'contact' mode AFM images revealed similar morphological characteristics, clearly emphasizing that the tooth enamel was not damaged during imaging.

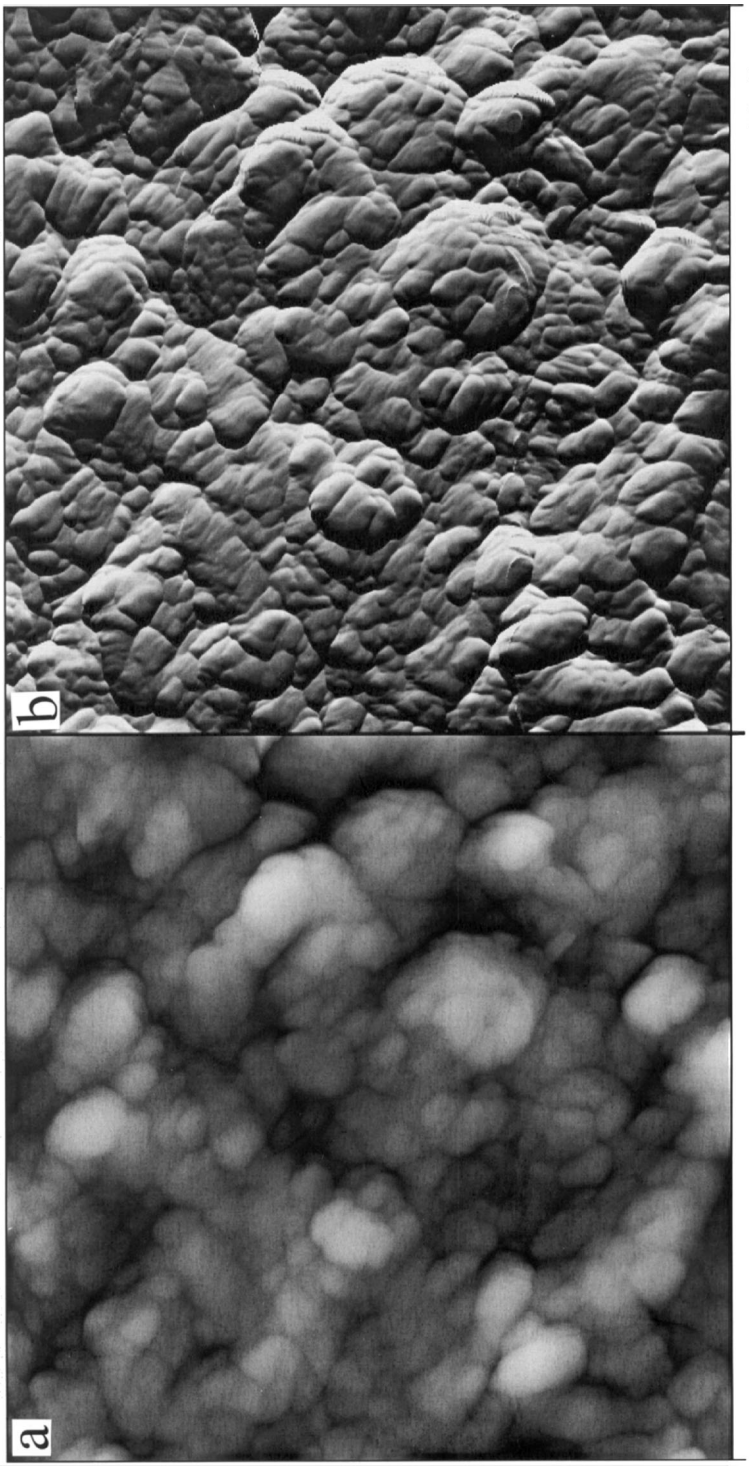

Figure 1. Top-view AFM tapping mode images of the healthy NA tooth, recorded in the 'height' (surface morphology) (a) and 'amplitude' (b) mode clearly reveal the distribution, size, and shape of numerous closely packed grains at the outer enamel surface.

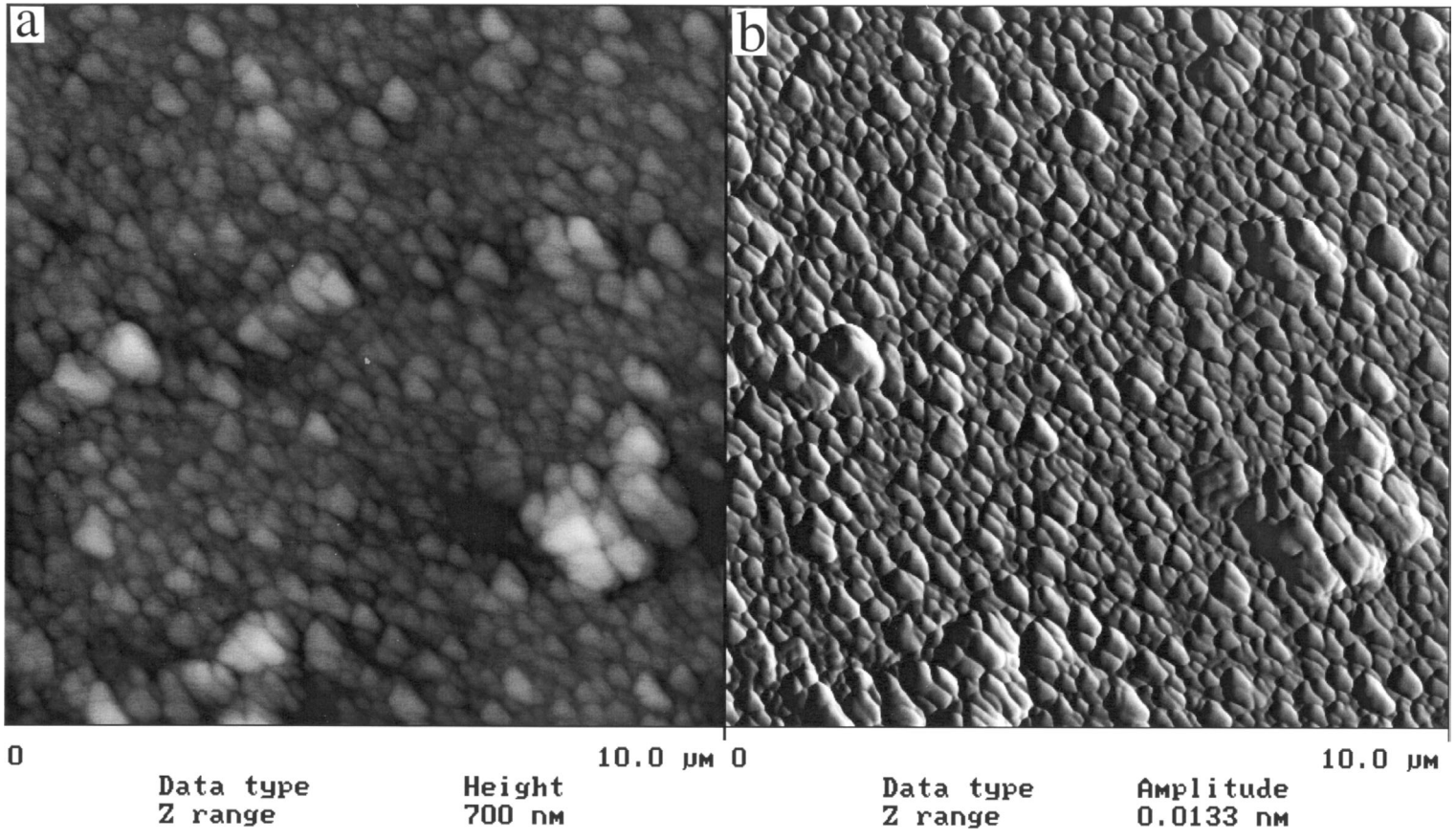

Figure 2. Top-view AFM tapping mode images of the healthy NC tooth, recorded in the 'height' (surface morphology) (a) and 'amplitude' (b) mode show a smooth and uniform top layer of the apatite distributed on the outer enamel surface.

AFM surface morphology analysis of the tooth enamel afflicted by amelogenesis imperfecta *(AI)*

Although we analyzed the surface morphological characteristics from the teeth of an adult and children (AI), we present only AFM images of the tooth of the child with AI. This is because we found that both possess very similar, or rather the same, typical morphological characteristics. As can be seen in the images in Fig. 3 [tapping mode imaging with presentation in (a) 'height' and (b) 'amplitude' modes], the outer enamel surface of the AI tooth is completely different from that observed from the NC tooth. In general, it is a rather uniform and flat surface with a RMS (Rq) of only 2.5 nm, without large aggregated grains but with high porosity. Indeed, the outer enamel layer consists of small (50–65 nm in diameter) irregularly displaced apatite grains with numerous pores (diameter 3–50 nm) forming an unusual network all over the top of the tooth surface. In particular, images recorded in the so-called 'amplitude' mode afford a better visualization of this peculiar ultrastructure of the AI tooth surface morphology. More details regarding the grain interconnections from the AFM image are presented in Fig. 4. Small and very uniformly structured grains are very loosely connected to each other, with a considerable empty space between them.

Figure 5 shows a high-resolution 3D AFM image, with small and well-defined individual grains incorporated in the porous network. We assume that this is the major characteristic of the AI tooth morphology. It is obviously completely different from the healthy tooth, where grains grow in a closely packed formation and occasionally form aggregates (cf. the images in Figs 1a and 1b). The high degree of surface porosity is also the most likely reason why the AI tooth appears to be fragile and weak; this was particularly noticed during the imaging when excessive force was used (i.e. contact mode imaging).

According to these morphological findings, one can deduce that the actual influence of amelogenin as a major protein component of the extracellular matrix is on the development of dental enamel. It is hypothesized that amelogenin acts as an inhibitor during the enamel growth, which preferentially forces the formation of isolated apatite grains. This leads to the conclusion that during the enamel biomineralization process, proteins such as amelogenin are actually located on the apatite surface. Therefore study of the interaction of amelogenin and the enamel surface during the early stages of the biomineralization process will be of special interest. From our studies, the mechanism of AI remains unresolved. For a better understanding of the AI mechanism, more detailed visualization of the enamel structure and related proteins will be required.

AFM images of the normal adult tooth (NA) and the normal child tooth (NC) clearly reveal the compact packing between the apatite grains (Figs 1 and 2), which contrasts sharply with the AI-child tooth (Figs 3 and 4). The rather loosely connected network of apatite grains can be observed much more vividly in Fig. 5. The apatite crystal morphology in AI tooth enamel is clearly perturbed in the diseased state. The voids and the porous network observed in the present

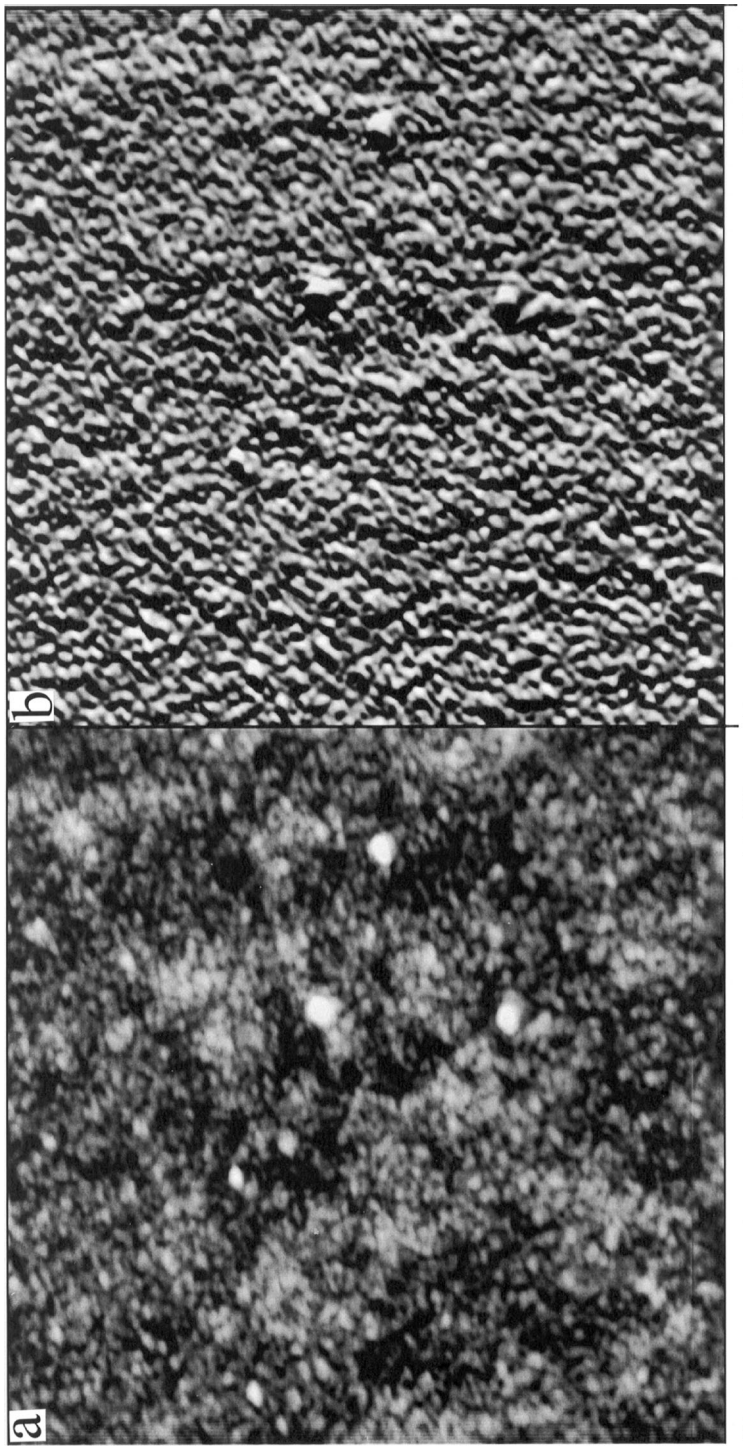

Figure 3. Top-view AFM tapping mode images of the tooth of the child with *amelogenesis imperfecta* (AI), recorded in the 'height' (surface morphology) (a) and 'amplitude' (b) mode clearly reveal high porosity and the existence of very small apatite grains.

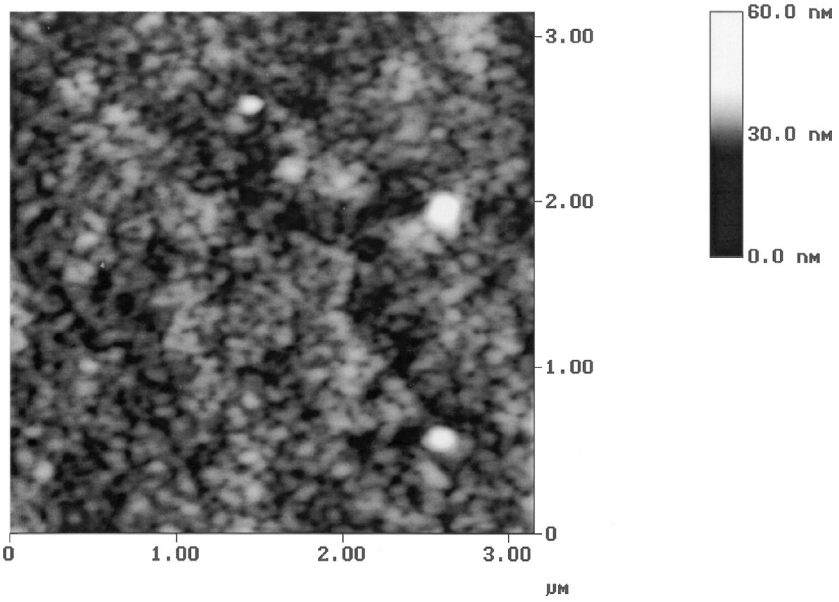

Figure 4. Top-view AFM (tapping mode) image of the AI-child tooth, recorded as 'height' (surface morphology) data, reveals the porous nature of the outer enamel surface.

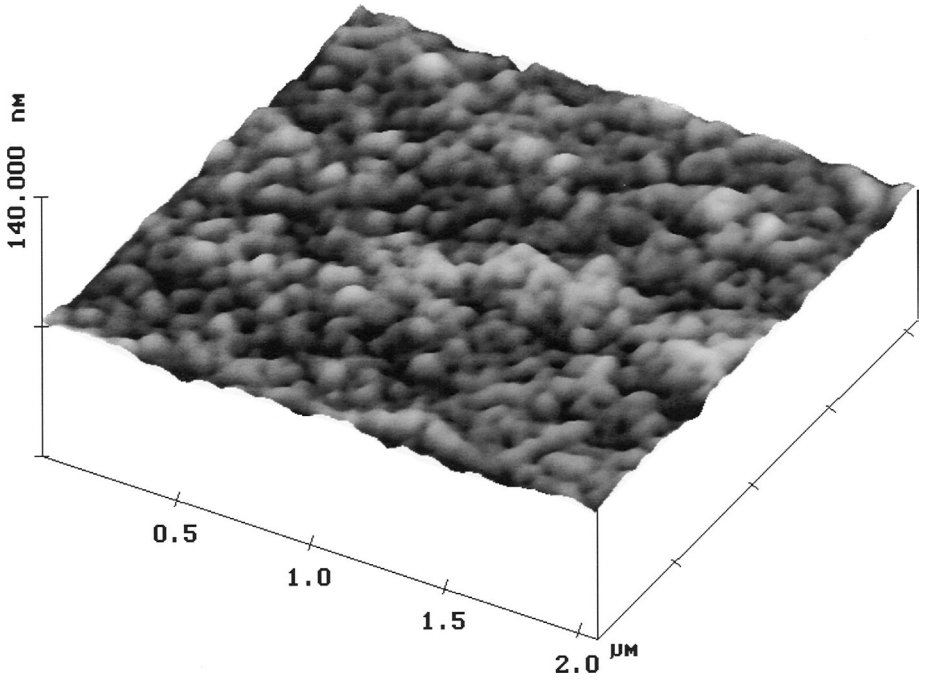

Figure 5. 3D presentation of the AFM image shows a loosely connected network of well-defined and mostly uniform individual grains on the enamel surface of the AI-child tooth.

study are very similar to the empty zones observed by Uzamis *et al*. [16] and earlier by Aldred *et al*. [14] using SEM on primary teeth samples afflicted by AI/hypoplasia. The most plausible explanation for the observations in the present study is the unequivocally poor mineralization in AI teeth. The voids probably result from defective protein synthesis by the ameloblasts. The disoriented pattern of HA crystallites seen in the AI tooth enamel presumably results from an altered primary, and hence secondary, structure of extracellular amelogenin through a cascade of events that are still poorly understood. The secondary structure of human amelogenin has not been reported in the literature. Nevertheless, from the earlier studies of Collier *et al*. [11] it was reported that the amelogenin gene responsible for X-linked AI undergoes the mutation of a conserved Pro to Thr and this presumably alters the 3D structure of human amelogenin. Further studies in order to gain more insight into the molecular basis of AI are in progress in our laboratories.

Acknowledgements

This research was partially supported by a grant from the National Institutes of Health (V. R.). V. R. acknowledges partial financial support from CONACyT during 1998–1999. V. R. expresses his grateful thanks to Dr. Daid Keith, Harvard School of Dental Medicine for consultations. N. B. was supported by CONACyT grants, 0913E-P and L0081-E9608.

REFERENCES

1. E. Strawich, P. H. Poon, V. Renugopalakrishnan and M. J. Glimcher, *FEBS Lett.* **184**, 188 (1985).
2. A. G. Fincham and J. M. Oldak, *Connective Tissue Res.* **32**, 119 (1995).
3. J. P. Simmer and M. L. Snead, in: *Molecular Biology of the Amelogenin Gene*, p. 59. CRC Press (1995).
4. V. Renugopalakrishnan, R. Garduño-Juárez, P. N. Casillas Lavín, J. C. Hernández Guerrero and K. Ilangovan, *Rev. Soc. Quim. Mexico* **43**, 24 (1999).
5. V. Renugopalakrishnan, E. S. Strawich, P. M. Horowitz and M. J. Glimcher, *Biochemistry* **25**, 4879 (1986).
6. S. Zheng, A. T. Tu, V. Renugopalakrishnan, E. Strawich and M. J. Glimcher, *Biopolymers* **26**, 1809 (1987).
7. V. Renugopalakrishnan, N. Pattabiraman, M. Prabhakaran, E. Strawich and M. J. Glimcher, *Biopolymers* **28**, 1823 (1989).
8. V. Renugopalakrishnan, M. Prabhakaran, S.-G. Huang, A. Balasubramaniam, E. Strawich and M. J. Glimcher, *Connective Tissue Res.* **22**, 131 (1989).
9. M. Prabhakaran, V. Renugopalakrishnan, B. Wilson, H. C. Cheung, E. Strawich and M. J. Glimcher, in: *Proteins: Structure, Dynamics, and Design*, V. Renugopalakrishnan, P. R. Carey, L. C. P. Smith, S. G. Huang and A. C. Storer (Eds), p. 202. ESCOM Science Publishers, Leiden (1991).
10. T. Ichio, Y. Yamashita and T. Terashima, *Bull. Tokyo Mod. Dent. Univ.* **39**, 71 (1992).
11. P. M. Collier, J. J. Sauk, J. Rosenbloom, Z. A. Yuan and C. W. Gibson, *Arch. Oral Biol.* **42**, 235 (1997).
12. C. J. Witkopf and S. Rao, *Birth Defects* **7**, 153 (1971).

13. B. Backman, G. Anneroth and P. Horstedt, *J. Oral Pathol. Med*. **18**, 140 (1989).
14. M. J. Aldred, P. J. M. Crawford, W. Rowe and R. P. Shellis, *J. Oral Pathol. Med*. **21**, 186 (1992).
15. M. Farina, A. Schemmel, G. Weissmuller, R. Cruz, B. Kachar and P. M. Bisch, *J. Struct. Biol.* **125**, 39 (1999).
16. M. Uzamis, H. Celik, N. Erkmen and Y. Batirbaygil, *J. Clin. Pediatr. Dent.* **21**, 265 (1997).
17. J. H. Kinney, M. Baldouch, G. W. Marshall and S. J. Marshall, *Arch. Oral Biol*. **38**, 1103 (1993).
18. M. Sarikaya, H. Fong and M. Snead, in: *Electron Microscopy*, Vol. III, p. 243 (1998).
19. S. N. Maganov and M.-H. Whangbo, in: *Surface Analysis with STM and AFM*. VCH Verlag, Weinheim (1994).
20. M. T. McDermott, C. A. McDermott and R. L. McCreery, *Anal. Chem*. **65**, 937 (1993).
21. R. J. Phillips, T. D. Golden, M. G. Shumsky and J. A. Switzer, *J. Electrochem. Soc*. **141**, 2391 (1994).
22. D. Aubach and Y. Cohen, *J. Electrochem. Soc*. **143**, 3525 (1996).
23. Y. G. Li and A. Lasia, *J. Appl. Electrochem*. **27**, 643 (1997).